www.ptcer.pl/mccm

MATERIAŁY CERAMICZNE /CERAMIC MATERIALS/, 62, 3, (2010), 355-362

Development and Mechanical Characterization of Hydroxyapatite Micro/Macro-Porous Scaffolds by an Innovative Gel-Casting Process

Paola Palmero[1]*, Mariangela Lombardi[1], Laura Montanaro[1], Jacopo Tirillò[2]
Cecilia Bartuli[2], Teodoro Valente[2], Paolo Marcassoli[3], Marina Cabrini[3]

[1] Dept. SMIC, Politecnico of Torino, INSTM – R.U. PoliTO – LINCE Lab., Torino, Italy
[2] Dept. ICMA, Sapienza University of Rome, INSTM R.U. Roma La Sapienza, Rome, Italy
[3] Dept. of Design and Technology, University of Bergamo, Dalmine (BG), Italy
*e-amil: paola.palmero@polito.it

Abstract

An innovative gel-casting process was developed in order to obtain micro and macro porous hydroxyapatite ($Ca_{10}(PO_4)_6(OH)_2$, HA) scaffolds to be used in regenerative medicine for bone tissue reconstruction. The micro-porous materials were prepared using HA suspensions having different solid loadings (in the range of 55-60 wt%) and gelling agent contents (in the range of 0.3-0.75 wt%). After the set-up of the operative parameters, macro-porous components were also prepared by using commercial polyethylene spheres (PE), sieved in the range 355-420 μm, as a fugitive agent, added to the ceramic suspensions before casting. The PE amount was fixed for obtaining a porosity of 60 vol.% in the fired materials. The mechanical investigation was carried out on both dense and porous samples. The compressive tests, 4-point bending tests and micro-hardness measurements were performed in order to determine Young's modulus, compressive strength, ultimate tensile stress and fracture toughness. Good correlations between mechanical properties were found. The results obtained for micro and macro-pororous specimens were related with a model based on the ideal cell. An extensive microstructural characterization was carried out by SEM and coupled to mechanical data in view of the validation of modelling tools based on DIB-FEA (digital image based finite element analysis) procedures.
Keywords: Hydroxyapatite, Micro/macro-porous scaffolds, Mechanical properties, DIB-FEA

ROZWÓJ I CHARAKTERYSTYKA MECHANICZNA MIKRO/MAKRO-POROWATYCH RUSZTOWAŃ HYDROKSYAPATYTOWYCH OTRZYMANYCH ZA POMOCĄ INNOWACYJNEGO PROCESU ODLEWANIA ŻELOWEGO

Rozwinięto innowacyjny proces odlewania żelowego w celu otrzymania mikro i makroporowatych rusztowań hydroksyapatytowych ($Ca_{10}(PO_4)_6(OH)_2$, HA) przeznaczonych do wykorzystania w medycynie regeneracyjnej do rekonstrukcji tkanki kostnej. Mikro-makro porowate materiały przygotowano przy wykorzystaniu zawiesin HA o różnej zawartości fazy stałej (w zakresie 55-60 % wag.) i czynnika żelującego (w akresie 0.3-0.75 % wag.). Po ustaleniu obowiązujących parametrów, makrporowate komponenty zostały przygotowane z wykorzystaniem komercyjnych kul polietylenowych (PE), wysianych w przedziale 355-420 μm, jako uchodzący składnik, dodawany do zawiesin przed odlewaniem. Ilość PE została ustalona tak, aby w wypalonych materiałach otrzymać porowatość wynoszącą of 60 % obj. Badania właściwości mechanicznych przeprowadzono na próbkach zarówno gęstych, jak i porowatych. Przeprowadzono testy ściskania, 4-punktowego zginania i pomiary mikrotwardości, aby oznaczyć moduł Younga, wytrzymałość na ściskanie, ostateczną wytrzymałość na zginanie i odporność na pękanie. Stwierdzono dobrą korelację pomiędzy właściwościami mechanicznymi. Wyniki uzyskane w przypadku mikro- i makroporowatych próbek powiązano z modelem opartym na komórce idealnej. Przeprowadzono obszerną charakterystykę mikrostrukturalną za pomocą SEM w odniesieniu do wyników badań właściwości mechanicznych w celu oceny poprawności narzędzi modelujących opartych na procedurze DIB-FEA (*digital image based finite element analysis* – odwzorowanie cyfrowe oparte na analizie elementów skończonych).
Słowa kluczowe: hydroksyapatyt, mikro/makroporowate rusztowanie, właściwości mechaniczne, DIB-FEA

1. Introduction

Calcium phosphate-based materials are currently used as bone substitute materials in modern heath care industry due to their low density, chemical stability, high wear resistance and compositional similarities to the human bone [1-2].

Calcium phosphate exists in different phases; however, at the temperature and pH of body fluids, hydroxyapatite ($Ca_{10}(PO_4)_6(OH)_2$, HA) is the most stable one [3]. In addition, the surgical implants usually should have complex shapes; among the various manufacturing techniques existing today, gelcasting is of great interest since it allows complex shaping, uniform structure and high strength, as required for clinical applications [4-5]. When tissue engineering is concerned, three-dimensional porous scaffolds with a highly interconnected porosity are designed, in order to allow cell migration, vascularization and diffusion of nutrients [6]. The ideal scaffold should have 50-95 vol.% of porosity, with diameters of hundred of microns and a number of interconnections, thus to achieve the bioresorption of the scaffold and the

subsequent new bone formation in the shortest time. In fact, macro-pores (150-400 μm) play an important role in cellular and bone ingrowth; micropores (few microns) can interact with protein and are mainly responsible for bioactivity [6]. The elaboration of such macro-porous materials with mechanical performances close to those of human bone is still a challenge. In fact, bone presents a dual structure, made by a dense cortical layer and a highly porous inner (named cancellous) part [7]. When compared to human cancellous bone, the macro-porous hydroxyapatite scaffolds exhibit comparable compressive strength, but poor resistance under tensile and shear stresses [8].

In this paper, micro and macro-porous hydroxyapatite scaffolds have been produced by a modified gelcasting process [9-11]. The innovation derives from the combination of conventional gelcasting procedure with the use of a sacrificial template, *i.e.* polyethylene spheres, as pores formers. As a gelling agent, an environmentally-friend biopolymer, such as agar [12], was selected. The produced scaffolds have been submitted to microstructural and mechanical characterization and data correlated to microstructural features.

2. Experimental

A commercially available (Plasma Biotal Ltd., U.K., Captal S), hydroxyapatite powder (HA) was used as a starting material. It is a highly crystalline and pure powder, just containing traces of calcium phosphate and alpha calcium orthophosphate, as declared by the supplier [13].

HA was calcined in the 1250-1500°C temperature range (heating rate of 10°C/min, 1 h soaking at the maximum temperature); X-ray diffraction (XRD) analyses were collected on as-received and calcined powdered samples with a Philips PW 1710 diffractometer using Cu Ka radiation (1.541874 Å), in the range 10-55°2θ, with a step size of 0.05°2θ and an acquisition time per step of 5 s.

HA aqueous suspensions were prepared at solid loading of 65 and 70 wt% (which correspond to 37.0 and 42.5 vol.%) respectively, by adding a commercially available dispersant (Duramax D-3021, ammonium salt of polycarbossilic acid). Dispersion was carried out under the magnetic stirring up to 24 h; the agglomerate size distribution as a function of dispersion time was followed by the laser granulometer, while the suspension pH was continuously monitored by a pH-meter.

High purity Agar (Sigma, A7049) was selected as gelling agent; it is a polysaccharide constituted by chains of glycosyl unites [12]. Agar was dissolved in distilled water, at 90°C, to yield a stock solution at 2 wt%. It was then cooled down to 60°C and added in a suitable amount to the dispersed ceramic slurries, kept at the same temperature. As a result, six different HA suspensions were yielded, with two solid loading (60 and 55 wt%) and three agar contents (0.3, 0.5 and 0.75 wt%, with respect to total water). For the sake of clarity, in Table 1 the six slurries are designated on the ground of HA solid loads (SL) and agar content (A). In addition, the quantity of HA powder, water, agar and dispersant used in each preparation are collected.

The obtained suspensions were cast into PMMA cylindrical moulds having the internal diameter of 14 mm and height of 40 mm. In order to remove air bubbles entrapped in the ceramic suspensions, cast was carried out under vacuum (at about 10^{-2} Pa). Gelation of the samples occurred during slow cooling to room temperature. The gelled pieces were de-molded after one day and dried in controlled humidity conditions for about 1 week.

For the development of porous samples, polyethylene spheres (PE, supplied by Clariant Italia SpA), sieved in 355-425 μm range, were used as a fugitive phase. The DTA-TG curves of PE is reported in Fig. 1, showing that decomposition is almost complete at 550°C. Such thermal–gravimetric curves were also exploited to set up the firing cycle of the porous materials, as described in the following. In Fig. 2, a SEM micrograph of the sieved PE fraction is shown: it can be observed the presence of several PE spheres with the size lower than 355 μm, probably due to their electrostatic adhesion to the bigger ones during sieving.

Table 1. Suspension designations related to the solid load (SL) and agar content (A): amount of HA, water, agar and dispersant used in each preparation.

	SL55-A03	SL60-A03
HA [g]	100	100
Water [g]	81.82	66.67
Agar [g]	0.245	0.2
Dispersant [g]	0.64	0.64
	SL55-A05	SL60-A05
HA [g]	100	100
Water [g]	81.82	66.67
Agar [g]	0.409	0.333
Dispersant [g]	0.64	0.64
	SL55-A075	SL60-A075
HA [g]	100	100
Water [g]	81.82	66.67
Agar [g]	0.614	0.5
Dispersant [g]	0.64	0.64

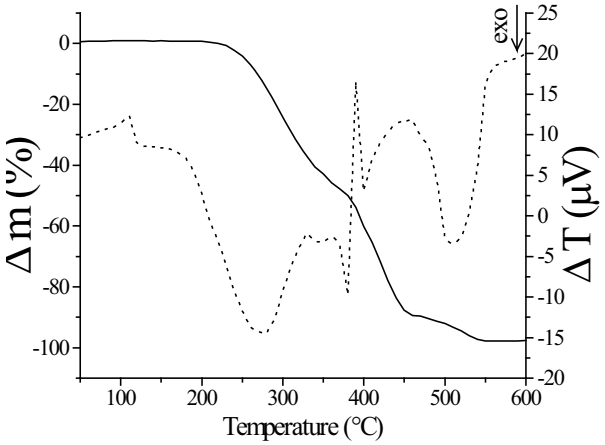

Fig. 1. DTA-TG curves of PE.

A SL60-A075 suspension was also prepared for the development of macro-porous components. This slurry was mixed to a fixed PE amount in order to obtain a porosity of 60 vol.% in the fired materials.

The gelcast green bodies were sintered up to 1300°C for 3 h (at a heating rate of 2°C/min). However, the PE-containing samples were submitted to a more complex low-temperature

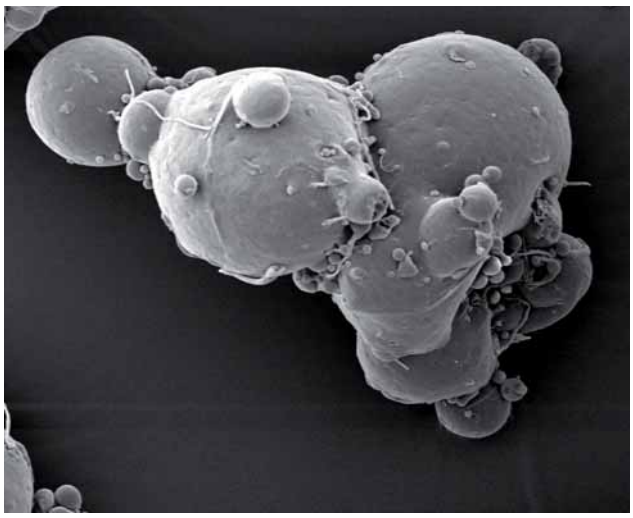

Fig. 2. SEM micrograph of sieved PE.

cycle (up to 600°C), made of several isothermal steps, set up in order to allow the burn-out of the fugitive phase without damaging the green ceramic structure.

Green and fired densities of the gelcast components were evaluated by weight and geometrical measurements.

The fired microstructures were observed by scanning electron microscopy (FEI SEM XL40), after careful optimization of the polished sections preparation procedures. For dense materials, homogeneous and compact microstructures were evidenced, with small amounts of residual microporosity in the correspondence of triple points (with an average size of about 500 nm - 1 μm, Fig. 3). A limited number of isolated defects was also identified, in the shape of irregular or spherical pores. A typical microstructure of the optimized cellular material, obtained after decomposition of 60 vol.% porogen spheres and final sintering, is shown in Fig. 4. A very good dispersion of macro-pores was achieved, and a compact and homogeneous microstructure of the dense (micro-porous) material was maintained during the gas species escape and high temperature densification. The presence of cracks, both radial and concentrical, around the spherical pores, is very limited.

The tests to evaluate the compressive modulus and strength were carried out by means of an hydraulic machine with a 25 kN load cell for macroporous specimens and 100 kN for microporous specimens. The tests were performed under displacement control at 0.1 mm/min rate. Before testing, specimens were polished in order to have regular surfaces, perpendicular to the main axis, with a h/d ratio in the range 1.5-2. Due to different cross sections along cylinders, stress was calculated using the minimum diameter.

Strain gages (120 ohm, 3 mm base for microporous specimens and 0.6 mm base for macroporous specimens) were applied with a cyanoacrylate-based glue on the lateral surface of each specimen, in order to measure strain. Preliminary loading/unloading tests were performed to set up calculation of modulus. Stress vs strain curves, compressive modulus, stress at break point and maximum stress were obtained.

Four point bending tests were also performed according to ASTM standard C1161-02c by means of an electro-mechanical machine with a 2.5 kN load cell in order to evaluate

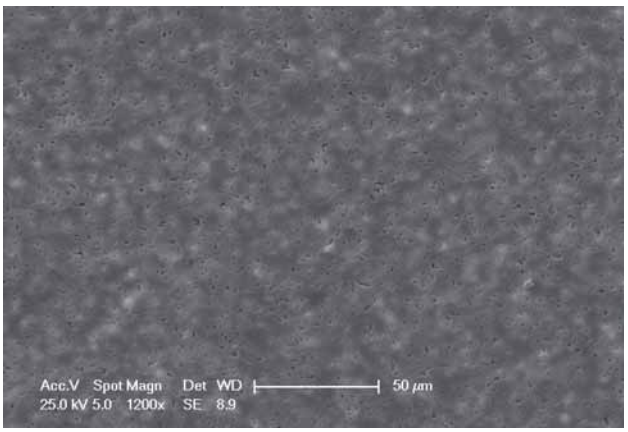

Fig. 3. Microstructure of a dense (micro-porous) HA material (SEM).

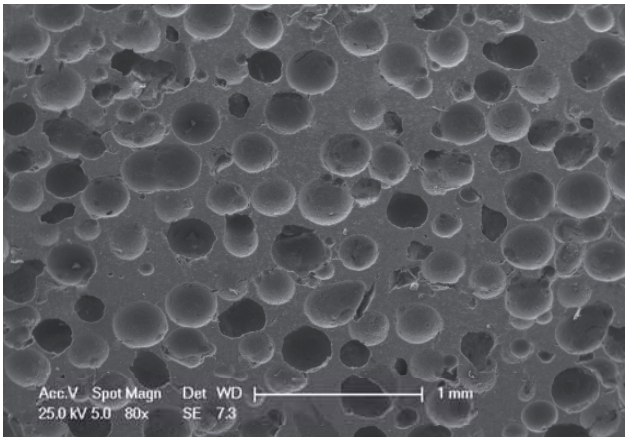

Fig. 4. Representative cross section of a cellular (60 vol.% PE spheres) HA material (SEM).

the modulus and strength.

Vickers microhardness tests were performed on dense samples, polished with abrasive papers till 2400 grit, avoiding any damage. The tests were performed with load of 1 kG and dwell time of 15 s. Fracture toughness in terms of K_{Ic} was calculated with the model proposed by Blendell [14], based on the value of microhardness and the dimensions of indentations and cracks at vertices. This method is in good agreement with the models found in literature and its results are very similar to those obtained with four point bending tests on notched specimens.

With the aim of reducing as much as possible, the time- and material-consuming experimental activity that would be necessary for the acceptance of multiple lots of cellular materials, produced with different amounts and distribution of macro and micro-porosity, a simulation of the mechanichal behaviour of macro-porous structures based on the results of the experimental activity was carried out. A digital-image based finite element analysis (DIB-FEA) [15-17] was applied to gel-cast cellular scaffolds. Such an approach allows a FE model to be built up that includes all the relevant microstructural features of a material (distribution of pores, presence of isolated defects, micro-cracks…) starting directly from real digital micrographs of its cross-sections. A simulation of the mechanical behavior or real components can thus be carried out on the designed model.The typical procedure for carrying out a digital image-based finite element analysis can be divided in the following steps:

i. choice of a representative cross-section;
ii. discretization of the domain corresponding to the imported digital image;
iii. identification of the different phases, optimization of the mesh and assignement of material properties;
iv. setting of boundary conditions and loads, followed by the solution.

The fields were computed with linear shape functions (element edges with nodes only at the end points were used). Finite elements analysis provides stress distribution and the attended value of elastic modulus calculations must be validated by comparison with the experimental mechanical tests.

3. Results and discussion

The as-received HA powder is pure hydroxyapatite, as shown by the XRD pattern of Fig. 5 (curve A). However, when calcined at high temperature, the secondary phases are yielded. Precisely, at 1250°C and 1300°C (curve B in Fig. 5), the β-$Ca_3(PO_4)_2$ (β-TCP) phase was clearly detected; when calcined at 1500°C (for 1 h), a partial transformation of the β-TCP into α-$Ca_3(PO_4)_2$ (α-TCP) also occurred, yielding a mixture of HA, β-TCP and α-TCP.

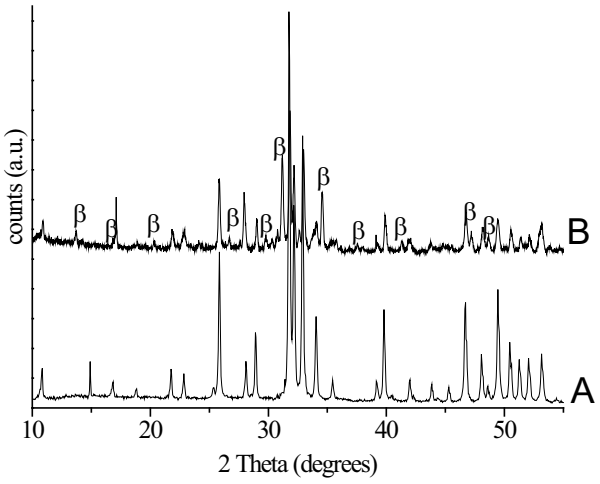

Fig. 5. XRD pattern of as-received HA (A) and after calcination at 1300°C for 1 h (B).

The presence of such secondary phases can affect the mechanical behaviour of pure HA-materials, as reported in literature [4, 18, 19]. β- and α-TCP reinforced HA composites have been already developed, showing the improved bending strength and fracture toughness as compared to pure hydroxyapatite [19]. In contrast, the Young's modulus was decreased by such phases [18]; according to the very few results that may be found for b-TCP, the elastic constant appears to be lower than that of HA [4]. In addition, such composites are highly biocompatible, as demonstrated by cell culture studies, using a human osteosarcoma cell line [20].

In Fig. 6, the cumulative distributions (vol.%) of the as-received powder and of the 24-h dispersed suspension are reported. Magnetic stirring is effective in reducing powder agglomeration. The agglomerate size corresponding to 50 % of particles population (d_{50}) was about 4 and 1.4 μm for the as-received and dispersed powders, respectively.

In Table 2, the green and final densities of the PE-free gelcast pieces are collected. These values are in partial agreement with literature data, showing that the higher the solid loading and the lower the gelling agent content, the higher is the green density [21]. In the present work, an increase of solid loading clearly corresponds to a higher green density. In contrast, the green values of 0.3 and 0.75-agar containing samples were similar, and the highest values were obtained in the materials with 0.5 wt% of agar, suggesting the intermediate gelling agent content as an optimum value.

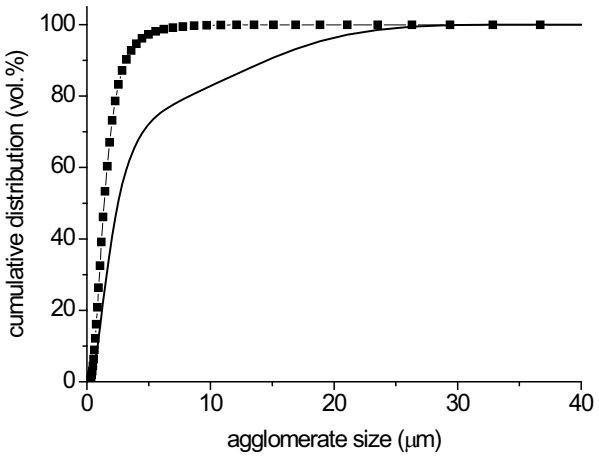

Fig. 6. Cumulative distribution (vol.%) vs. agglomerate size of as-received (solid line) and 24-h dispersed (squares) HA.

Table 2. Green and fired densities of the PE-free gelcast pieces.

	Green density [%TD]	Fired density [%TD]	
		average	st. dev.
SL55-A03	48.8	80.4	2.1
SL60-A03	49.4	81.0	4.1
SL55-A05	49.4	83.9	2.1
SL60-A05	50.9	84.5	8.4
SL55-A075	48.2	82.3	1.8
SL60-A075	49.1	83.9	1.0

The fired density is expressed as % of the theoretical value for pure hydroxyapatite (3.16 g/cm^3), in spite of the significant β-TCP phase formed after sintering at 1300°C (see Fig. 5). However, its theoretical density value is quite close to that of HA (3.07 g/cm^3 [22]), so that an overall theoretical value of 3.16 g/cm^3 can be reasonably assumed.

The results of compressive tests showed a high scattering of results. The differences between samples produced with different compositions are very small with respect to the deviation of the values. For this reason they were analyzed in terms of cumulative distribution curves.

Figs. 7 and 8 show the cumulative frequency of the compressive modulus and the stress value at the first break point, respectively. By comparing the distributions, the highest differences were found between the specimens obtained with 0.3 agar content and the other specimens, with a lower effect of the solid load content. In general, the compressive modulus values seem to increase as the agar quantity increases, but the highest values (over 100 GPa) were measured with the intermediate agar content for the samples produced

with 55 solid load. No evident effect of the solid load can be pointed out for stiffness under compressive loading.

The values of stress at the break point confirm the general trend observed for the compressive module. The scattering of results is very evident, particularly as the mechanical properties increase. The specimens with a higher solid load show a higher compressive strength, for the same agar content. By comparing the samples with the same solid load, an increase in mechanical strength seems to be associated with a higher agar content, but this trend was not confirmed by the sample with 60 s.l. and 0.5 agar which shows a behaviour similar or slightly better than the sample with 0.75 agar.

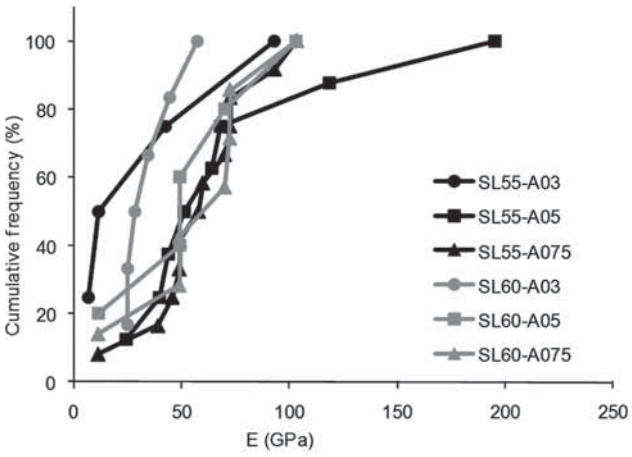

Fig. 7. Cumulative distributions of compressive modulus of microporous specimens.

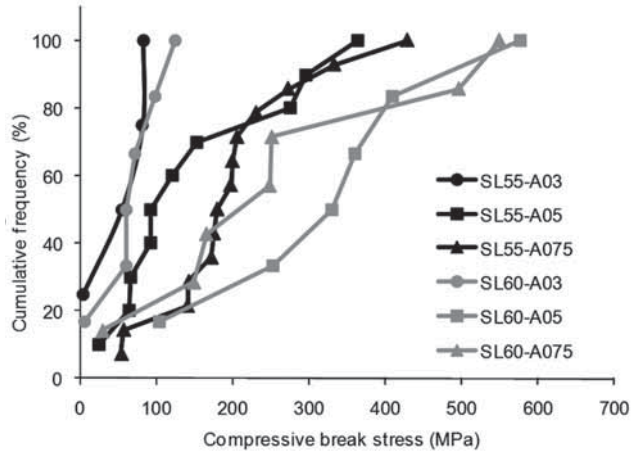

Fig. 8. Cumulative distributions of compressive stress at break point of microporous specimens.

The average results are summarized in Table 3. Fig. 9 shows the compressive modulus vs. break stress. As expected, high stiffness is associated with high strength, but the trend seems to be non-linear.

Compressive stiffness and strength show a strong relation with the microstructural properties of gelcast material, in particular density (Fig. 10). Nevertheless, it is necessary to point out that apparent density values can be affected by different microporosity and the presence of defects in the lattice, hiding the real conditions of the material. The defect can influence the break stress, so a good microstructural characterization and fracture toughness analysis are crucial anyway. The presence of such defects can also explain the high scattering of results. Pores or other defects were in some cases observed on fracture surfaces.

The results of four point bending tests performed on dense specimens in the shape of prismatic bars can be summarized as follows: elastic modulus is 58.9 ± 1.7 GPa, flexural strength is 35.7 ± 2.6 MPa.

Table 3. Summary of compressive test results of microporous specimens.

	E, [GPa]	σ_{break}, [MPa]	σ_{max}, [MPa]
SL55-A03	38.5	56.1	86.7
SL60-A03	39.7	83.6	101.3
SL55-A05	74.7	195.6	245.1
SL60-A05	64.6	386.5	398.6
SL55-A075	72.1	223.4	281.9
SL60-A075	61.2	270.1	316.3

Table 4 summarizes the Vickers microhardness and K_{Ic} values obtained. No evident correlation was found for microhardness with microstructural or other mechanical properties. Fracture toughness values are similar to those reported in literature. Under equal defect dimension conditions, the compressive strength and stress intensity factor are directly proportional. However, the variation of K_{Ic} is indeed very low and it can be assumed to be about constant. Thus the variation of break stress can be explained only with a different dimension of defects, confirming the relation between microstructure and behaviour under loading.

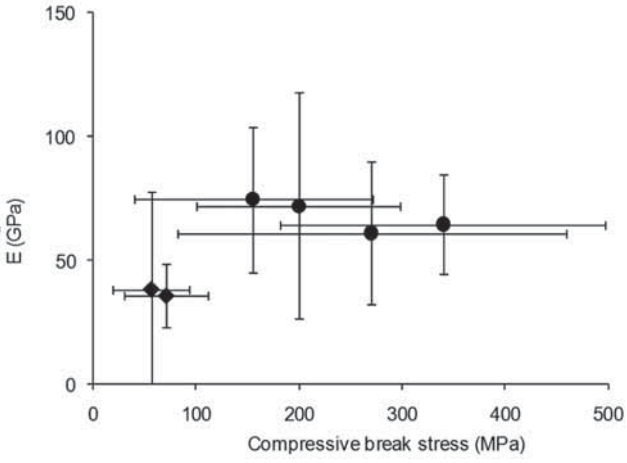

Fig. 9. Compressive break stress vs compressive modulus of the microporous specimens.

Table 4. Summary of microhardness and fracture toughness results of microporous specimens.

	$HV_{1000,15}$	K_{Ic} [MPa√m]
SL55-A03	226	0.86
SL60-A03	238	0.81
SL55-A05	187	1.18
SL60-A05	241	1.52
SL55-A075	203	1.45
SL60-A075	210	0.97

The results of compressive tests of macroporous samples are shown in Table 5. By increasing the solid load from 60 to 62, a slight increase in compressive strength and stiffness was observed. The compressive modulus is about ten times lower than that obtained with microporous samples. The compressive strength is very low due to high porosity, necessary to ensure good biocompatibility. The fracture mechanism is very different from that observed for microporous samples. In that case a brittle fracture favoured by pores or defects was found. In the case of macroporous samples the collapse of cells due to flexural stresses on walls and propagation of cracks from pore to pore were observed (Fig. 11).

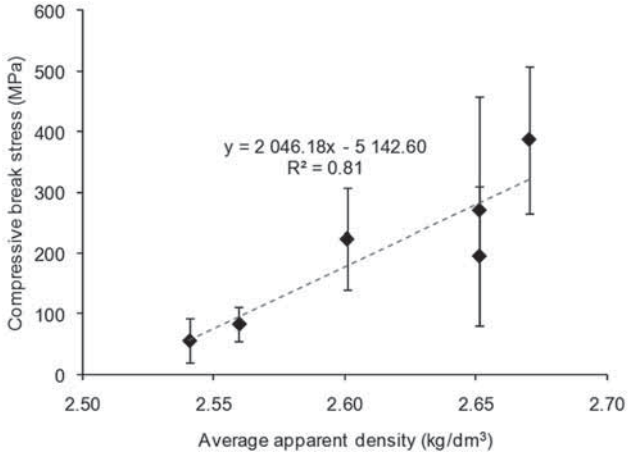

Fig. 10. Compressive break stress of the microporous samples (s.l. 55/60, agar 0.3/0.5/0.75) as a function of the average apparent density.

Table 5. Summary of mechanical results of macroporous specimens.

	E [GPa]	σ_{break} [MPa]	σ_{max} [MPa]
SL60-A075	7.01	4.10	4.10
SL62-A075	7.23	5.11	6.11

As already found for microporous samples, good correlations between stiffness and compressive strength, between mechanical properties and apparent density were observed (Fig. 12).

For the correlation between mechanical properties of macroporous hydroxyapatite and the microporous one, the model of Gibson and Ashby was applied [23], based on an ideal cell with thickness of the cell walls t and the length of the walls L. According to the model, the relative density of a ceramic foam is calculated by

$$\frac{E}{E_s} = C_2 \cdot \left(\frac{t}{L}\right)^4 = C_3 \cdot \left(\frac{\rho}{\rho_s}\right)^2, \qquad (1)$$

where E and E_s are the compressive modulus of the foam and the wall, ρ/ρ_s is the relative density, ρ is the density of the foam, while ρ_s is the density of the cell wall. This was assumed equal to that of microporous specimens. According to Brezny, the range of validity of the equation is for C_3 values from 0.36 to 0.5 [24].

By considering the results obtained for the specimens with solid load of 60 and agar 0.75 and preliminary compressive test results obtained for the corresponding specimens with 60 % porosity, a C_3 value very close to the upper limit of the range by Brezny was found. The used average values and the value of C_3 are shown in Table 6.

Table 6. Application of the model proposed by Gibson and Ashby [20].

	Average values	
ρ	1.25	[kg/dm³]
ρ_s	2.64	[kg/dm³]
E	7.01	[GPa]
E_s	61.18	[GPa]
C_3	0.51	

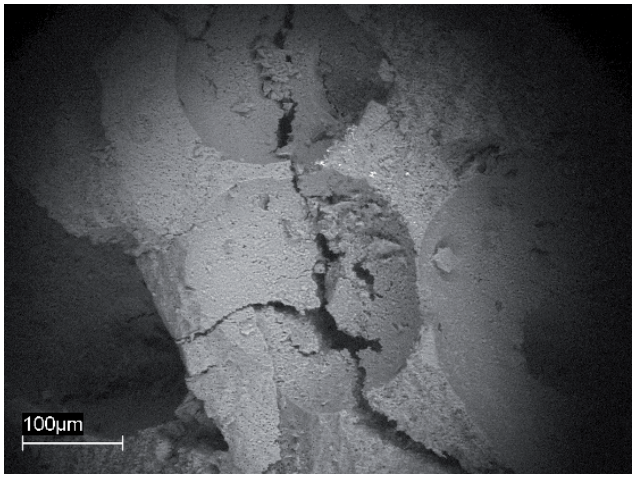

Fig. 11. Example of fracture surface of macroporous specimen after compressive test (SEM image).

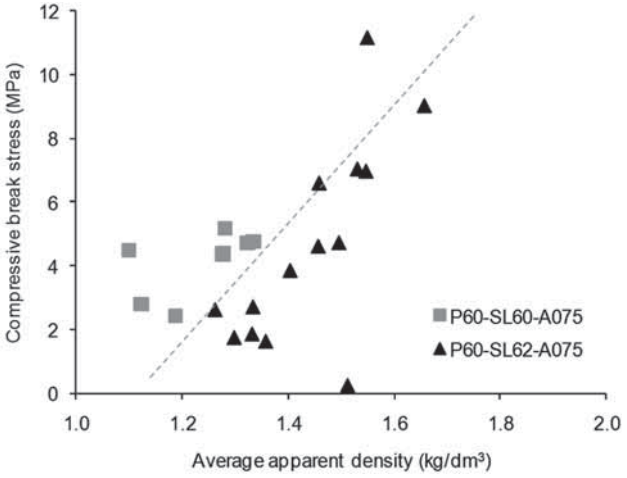

Fig. 12. Compressive break stress of macroporous samples as a function of apparent density.

The results of the finite element modeling can be resumed as follows. Using version 2 of the software OOF (Object Oriented Finite Element), devoloped by NIST (National Institute of Standards & Technology, USA) [25-26], computational meshes were generated from binary maps of selected representative images (Fig. 4) and iteratively refined to adapt them to the calculation requirements. A mesh made of 28225 elements and characterized by a total homogeneity (ratio between areas occupied in each element by the two phases) of 99.3 %, is shown in Fig. 13.

The experimental results of mechanical characterization carried out on dense (microporous) materials were used to

assign reliable values of the elastic modulus to the "black" phase for the simulation of cellular materials behaviour on compression. The following values were used for the FE analysis: E_{dense} = 61 GPa, ν (Poisson ratio) = 0.3.

The mechanical behaviour of macroporous HA ceramics was simulated (ABAQUS 6.7) assigning a fixed joint constraint to the lower surface and imposing a length variation of – 0.25 % to the mesh.

In Fig. 14, the distribution of nodal displacements throughout the cross section of the cellular specimen shown in Fig. 5 (artificially amplified for better visualization) is illustrated.

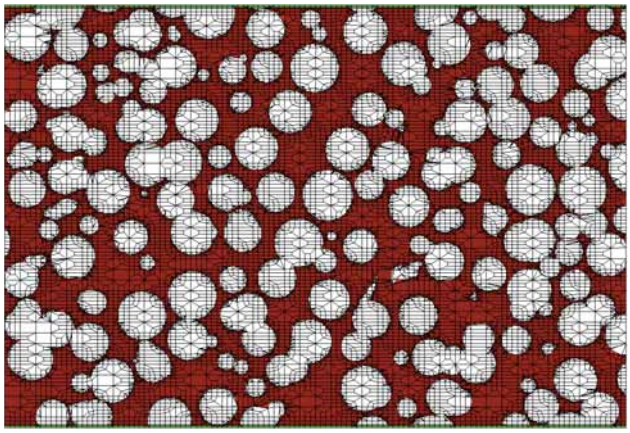

Fig. 13. Binarized digital image corresponding to the cross section shown in Fig. 4; the optimized mesh (28225 elements, 99.3 % homogeneity) is superimposed.

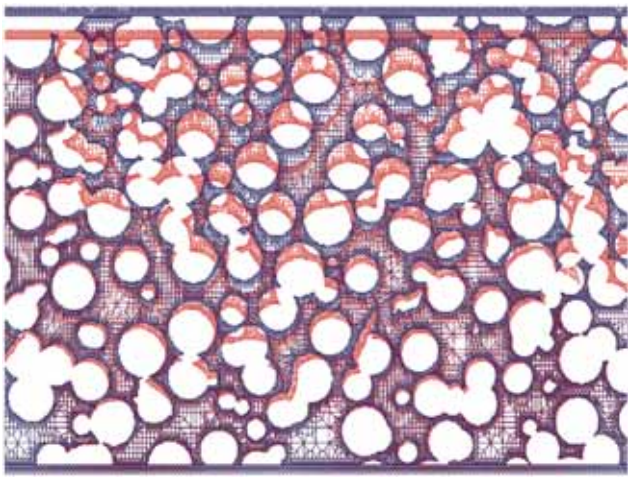

Fig. 14. Distribution of nodal displacements troughout the cross section of the cellular specimen, artificially amplified for better visualization (blue = original mesh; red = deformed mesh).

The model allowed plane strain values (ε_x and ε_y) to be calculated, in experienced in each node of the mesh. By substitution of the calculated deformations in the Hooke's law for plane strain (2):

$$E_{att} = \frac{\sigma_y \cdot (1+\nu)\cdot(1-2\nu)}{\nu\cdot\varepsilon_x + (1-\nu)\cdot\varepsilon_y} \qquad (2)$$

the attended elastic modulus of the cellular material can be obtained. For the present simulation, a value of E_{att} = 2.4 GPa was calculated.

The distribution of the intensity of the stress, σ_{yy}, within the structure can also be evidenced (Fig. 15), confirming that the areas that develop the highest stresses as a consequence of the uniform application of an uniaxial load are those characterized by the thinnest walls among cavities.

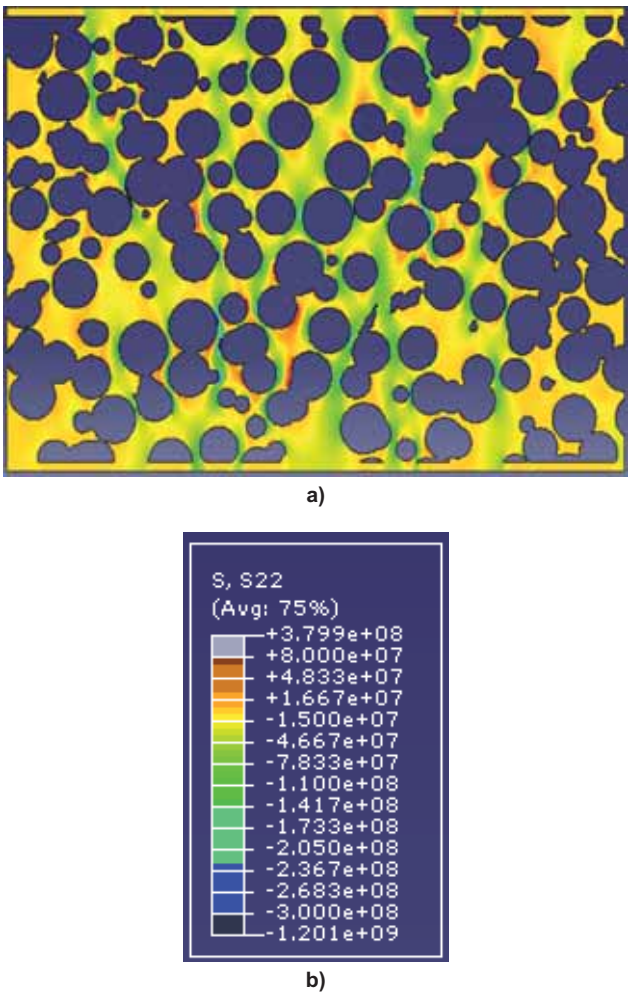

Fig. 15. Distribution of stresses in the direction of axial load (σ_{yy}): a) colorimetric map and b) scale legend.

4. Conclusions

The following conclusions can be drawn from experimental and modeling activities:

– ceramic materials obtained by gel casting of hydroxyapatite powders are characterized by about 15-20 vol.% residual microporosity from thermal degradation of the gelling agent and subsequent sintering of ceramic powders; an average elastic modulus of about 66.7 GPa, a compression resistance of about 279.8 MPa and fracture toughness of about 1.3 MPa$\sqrt{m}$ were measured for the samples obtained with different solid loads and volume % of agar, without the addition of pore forming agents;

– the amount, size and distribution of macroporosity of cellular ceramics can be controlled by correctly selecting the size of pore forming agents (polyethylene spheres) and by optimizing their dispersion in the gelling agent; about 60 % porous cellular materials could be obtained at the end of the optimization of gel-casting procedures,

with even distribution of mainly spherical cavities with diameters ranging from about 350 to 450 μm;
– DIB FEA simulation of the mechanical behaviour implemented starting from SEM micrographs of representative cross sections gave rise to quite reliable predictions of elastic properties; elastic moduli of the same order of magnitude were calculated for cellular ceramics from experimental testing and from simulation procedures.

A present limitation of the simulation procedure can be found in the practical impossibility (due to excessively onerous computing effort and to the limits in the resolution of digital images) of taking into account simultaneously, in one single calculation, microstructural features of different orders of magnitude, such as micropores deriving from incomplete sintering and macropores or other macro-defects generated by the presence of pore forming agents.

Certain advantages can be derived from the application of DIB-FEA methods to cellular materials by the possibility of creating direct real correlations between specific microstructural features and overall mechanical elastic properties, thus allowing the number of material developing cycles to be reduced.

Bio-compatibility of the described cellular materials could be strongly influenced not only by the morphology of the scaffolds (micro and macro-porosity) but also by their intrinsic structural resistance and brittleness. The investigations of the bio-compatibility of the produced HA scaffolds are presently being carried out, and results will be made available soon.

Acknowledgments

The authors wish to thank the Italian Ministry MIUR for having partially supported this research in the frame of the Project PRIN 2006 “Design and fabrication of organic, inorganic and hybrid nanostructured scaffolds as substrates for the differentiation of stem cells in regenerative medicine”.

References

[1] Ducheyne P., Qiu Q.: „Bioactive ceramics: the effect of surface reactivity on bone formation and one cell function”, Biomaterials, 20, (1999), 2287-2303.
[2] Ray C.: „Calcium phosphate biomaterials and bone mineral. Differences in composition, structure and properties”, Biomaterials, 11, (1990), 13-15.
[3] Hench L.: „Bioceramics”, J. Am. Ceram. Soc., 81, (1998), 1705-1728.
[4] Chen B., Zhang Z., Zhang J., Lin Q., Jiang D.: „Fabrication and mechanical properties of b-TCP pieces by gel-casting method”, Mater. Sci. Eng. C, 28, (2008), 1052-1056.
[5] Padilla S., Garia-Carrodeguas R., Vallet-Regi M.: „Hydroxyapatite suspensions as precursors of pieces obtained by gelcasting method”, J. Eur. Ceram. Soc., 24, (2004), 2223-2232.
[6] Sanchez-Salcedo S., Nieto A., Vallet-Regi M.: “Hydroxyapatite/b-tricalcium phosphate/agarose macroporous scaffolds for bone tissue engineering”, Chem. Eng. J., 137, (2008), 62-71.
[7] Nissan B.B.: „Nanoceramics in biomedical applications”, MRS Bull., 29, (2004), 28-32.
[8] Charriere E., Lemaitre J., Zysset Ph.: „Hydroxyapatite cement scaffolds with controlled macroporosity: fabrication protocol and mechanical properties”, Biomaterials, 24, (2003), 809-817.
[9] Tulliani J.-M., Naglieri V., Lombardi M., Montanaro L.: „Gel casting of porous alumina and zirconia bodies”, Adv. Tech. Mat. Mat. Proc. J., 11, (2009), 9-18.
[10] Lombardi M., Montanaro L., Gremillard L., Chevalier J.: „A modified gelcasting procedure to prepare alumina porous components: process optimization and preliminary mechanical tests”, Ceram. Eng. Sci. Proc., 29, (2008), 287-298.
[11] Lombardi M., Naglieri V., Tulliani J.-M., Montanaro L.: „Gelcasting of dense and porous ceramics by using a natural gelatine”,. J. Porous Mat., 16, 4, (2009), 393-400.
[12] Labropoulos K.C., Niesz D.E., Danfforth S.C., Kevrekidis P.G.: „Dynamic rheology of agar gels: theory and experiments. Part I. Development of a rheological model”, Carbohydrate Polymers, 50, (2002), 393-406.
[13] www.plasmabiotal.com
[14] Fischer H., Marx R.: „Fracture toughness of dental ceramics: comparison of bending and indentation method”, Dental Mater., 18, (2002), 12-19.
[15] Hollister S.J., Kikuchi N.: „Homogenization theory and digital imaging: A basis for studying the mechanics and design principles of bone tissue”, Biotechnol. Bioeng., 43, (1994), 586-596.
[16] Terada K., Miura T., Kikuchi N.: „Digital image-based modeling applied to the homogenization analysis of composite materials”, Comp. Mechan., 20, (1997), 331-346.
[17] Terada K., Hori M., Kyoya T., Kikuchi N.: „Simulation of the multi-scale convergence in computational homogenization approach”, Int. J. Sol. Struct., 37, 16, (2000), 2285-2311.
[18] Lopes M.A., Silvia R.F., Monteiro F.J., Santos J.D.: „Microstructural dependence of Young’s and shear moduli of P_2O_5 glass reinforced hydroxyapatite for biomedical applications”, Biomaterials, 21, (2000), 749-754.
[19] Lopes M.A., Monteiro F.J., Santos J.D.: „Glass reinforced hydroxyapatite composites: fracture toughness and hardness dependence on microstructural characterization”, Biomaterials, 20, (1999), 2085-2090.
[20] Lopes M.A., Knowles J.C., Santos J.D., Monteiro F.J., Olsen I.: „Biological evaluation of glass reinforced hydroxyapatite by flow cytometry”, Bioceramics, 10, (1998), 575-578.
[21] Olhero S.M., Tarì G., Coimbra M.A., Ferreira J.M.F.: „Synergy of polysaccharide mixtures in gelcasting of alumina”, J. Eur. Ceram. Soc., 20, (2000), 423-429.
[22] JCPDF n° 09-0169.
[23] Gibson L.J., Ashby M.F.: Cellular Solids: Structure and Properties, Pergamon Press, New York, 1988.
[24] Brezny R., Green D.J.: „Mechanical behavior of cellular solids”, Mater. Sci. Tech., 11, (1992), 467-516.
[25] Reid A.C.E., Langer S.A., Lua R.C., Coffman V.R., Haan S.I., Garcia E.: „Image-based finite element mesh construction for material microstructures”, Comp. Mater. Sci., 43, (2008), 989-999.
[26] Carter W.C., Langer S.A., Fuller E.R.: The OOF Manual: version 1.0, National Institute of Standards and Technology, NISTIR No. 6256, 1998.

♦

Received 29 April 2010; accepted 28 May 2010